

The coalescence of liquid drops in a viscous fluid: interface formation model

James E. Sprittles[†] and Yulii D. Shikhmurzaev

Mathematics Institute, University of Warwick, Coventry CV4 7AL, UK
School of Mathematics, University of Birmingham, Birmingham B15 2TT, UK

(Received 21 October 2013; revised 5 March 2014; accepted 29 May 2014;
first published online 24 June 2014)

The interface formation model is applied to describe the initial stages of the coalescence of two liquid drops in the presence of a viscous ambient fluid whose dynamics is fully accounted for. Our focus is on understanding (a) how this model's predictions differ from those of the conventionally used one, (b) what influence the ambient fluid has on the evolution of the shape of the coalescing drops and (c) the coupling of the intrinsic dynamics of coalescence and that of the ambient fluid. The key feature of the interface formation model in its application to the coalescence phenomenon is that it removes the singularity inherent in the conventional model at the onset of coalescence and describes the part of the free surface 'trapped' between the coalescing volumes as they are pressed against each other as a rapidly disappearing 'internal interface'. Considering the simplest possible formulation of this model, we find experimentally verifiable differences with the predictions of the conventional model showing, in particular, the effect of drop size on the coalescence process. According to the new model, for small drops a non-monotonic time dependence of the bridge expansion speed is a feature that could be looked for in further experimental studies. Finally, the results of both models are compared to recently available experimental data on the evolution of the liquid bridge connecting coalescing drops, and the interface formation model is seen to give a better agreement with the data.

Key words: breakup/coalescence, capillary flows, drops and bubbles

1. Introduction

Coalescence, which is the process of two liquid volumes merging into one, is central to numerous natural phenomena and a variety of technological applications of fluids (Kovetz & Olund 1969; Grissom & Wierum 1981; Dreher *et al.* 1999; Bellehumeur, Biaria & Vlachopoulos 2004). In order to develop these technologies, it is necessary to have a mathematical model of the process that would allow one to reliably describe its dynamics and hence minimize the time and resources on experimentation. The current trend towards miniaturization of the fluid volumes undergoing coalescence in various applications, e.g. in biotechnologies (Squires & Quake 2005; Seeman *et al.* 2012) and additive manufacturing (Derby 2010; Singh *et al.* 2010), makes it vital to accurately model the initial stages of coalescence

[†] Email address for correspondence: J.E.Sprittles@warwick.ac.uk

for which a mathematically singular description (Hopper 1984; Richardson 1992; Sprittles & Shikhmurzaev 2012a, 2014) would not be acceptable. The latter has been reinforced by recent experiments (Paulsen, Burton & Nagel 2011), which employed a new experimental technique that made it possible to probe the coalescence dynamics on the ‘microfluidic’ spatio-temporal scales inaccessible to traditional optical methods used so far (Wu, Cubaud & Ho 2004; Aarts *et al.* 2005; Thoroddsen, Takehara & Etoh 2005).

The experimental breakthrough achieved in Paulsen *et al.* (2011) made it possible to test various mathematical models of the process, and the first one to be tested was the ‘conventional’ model used in most studies (Eggers, Lister & Stone 1999; Duchemin, Eggers & Josserand 2003). This model assumes that coalescence takes place on a length scale below that of continuum mechanics, so that, from the viewpoint of continuum mechanics, at the very onset of the process, one already has a single body of fluid consisting of the two volumes that were brought into contact and a smooth, albeit infinitesimal, liquid bridge connecting them. This scheme implies an intrinsic singularity at the start of the process (Hopper 1984, 1990; Richardson 1992; Hopper 1993a,b) and, as was shown in a numerical study that considered the conventional model in its entirety (Sprittles & Shikhmurzaev 2012a), it fails to describe the newly available experimental data: the model strongly overpredicts the speed at which the bridge connecting the coalescing volumes expands. The situation was not remedied even when, for the first time, the dynamics of the viscous gas surrounding the coalescing volumes was fully accounted for (Sprittles & Shikhmurzaev 2014). This makes it worth while to examine how the conventional model could be generalized to incorporate some additional physics that would allow one to describe the coalescence process in a singularity-free way.

A generalization of the conventional model considered in Sprittles & Shikhmurzaev (2012a) is known as the interface formation model (Shikhmurzaev 2007). In the case of coalescence, this model suggests that, as two liquid volumes are pressed against each other, a part of the free surface becomes ‘trapped’ between them, forming an ‘internal interface’ (figure 1). This interface gradually (although, in physical terms, very quickly) disappears, losing its specific ‘surface’ properties, such as the surface tension, as the fluid particles forming this interface adjust to their new environment and turn into ‘ordinary’ bulk particles. When the disappearance of the internal interface separating the two volumes is complete, the coalescence as such is over, one has a single body of fluid with a finite-sized smooth bridge connecting the initial volumes, and the conventional model can take over without giving rise to any mathematical singularities associated with the ‘smooth but infinitesimal’ bridge it uses to start the process. Notably, before the internal interface disappears, the residual surface tension associated with it can sustain a (gradually disappearing) angle in the free surface, and, once the coalescence is complete and the residual surface tension is gone, the free surface becomes smooth, as required by the conventional model, which from that moment onwards can take over.

Simplifications outlined in §4 will allow us to consider the ambient fluid to be either a gas or a second immiscible liquid. Notably, it has already been shown that an ambient gas affects the flow described using the conventional model (Sprittles & Shikhmurzaev 2014), even at surprisingly small gas-to-liquid viscosity ratios, as the presence of the gas can qualitatively change the free-surface evolution in the early stages of the process, in particular suppressing the formation of a toroidal bubble anticipated by earlier studies (Oguz & Prosperetti 1989; Duchemin *et al.* 2003), where the ambient gas was regarded as inviscid and dynamically passive. Given that in the

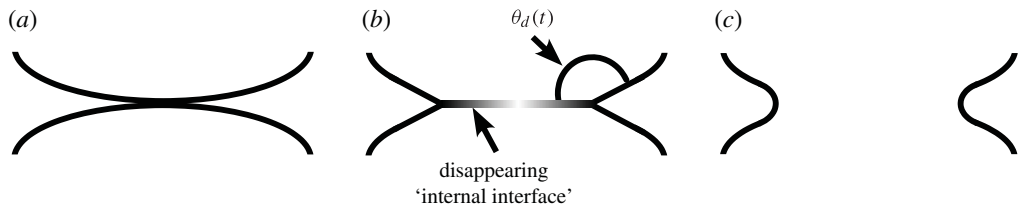


FIGURE 1. Sketch illustrating the scheme used in the interface formation/disappearance theory. The initial contact point (a) is followed by a fraction of the free surface being ‘trapped’ between the bulk phases, forming a gradually disappearing ‘internal interface’ (b), and, as the ‘internal interface’ disappears and the ‘contact angle’ θ_d , which is initially equal to 180° , relaxes to its ‘equilibrium’ value of 90° , the conventional mechanism takes over (c). The interface formation/disappearance model provides boundary conditions on interfaces, which are modelled as zero-thickness ‘surface phases’; these interfaces, including the ‘internal interface’ in (b), are shown as finite-width layers for graphical purposes only.

interface formation model there is a cusp formed when the volumes first touch, which then evolves into a corner, one may expect a different effect of the gas dynamics than in the case of the conventional model, where the interface is assumed to be smooth immediately after the onset of the process. This aspect will be investigated.

It has been shown (Sprittles & Shikhmurzaev 2012a) that the interface formation model’s predictions are in better agreement than the conventional model’s with the experimental data on the early stages of coalescence (Paulsen *et al.* 2011), and this fact justifies its further investigation. In Sprittles & Shikhmurzaev (2012a) only a direct comparison of theory with experimental data was provided, without any parametric study of the model, which will be rectified here by (a) investigating how the surface variables evolve and depend on the constants characterizing material properties of the liquid–fluid system, (b) considering the effect of the ambient fluid on the coalescence process and (c) determining the coupling between the dynamics of the interfaces and that of the ambient fluid. The main emphasis throughout will be on highlighting the specific features of the coalescence process, as described by the interface formation model, that distinguish it from the conventional model, with experimental verification of these effects in mind. Only once this has been achieved will we consider a comparison to the experimental data with the effect of the ambient gas now fully accounted for.

2. Problem formulation

Consider the axisymmetric coalescence of two drops that are grown from two syringes and start coalescing when each of them reaches the shape of a hemisphere (figure 2). Both the liquid forming the drops and the ambient fluid, whose dynamics we will also take into account, will be described as incompressible Newtonian fluids with constant densities ρ , ρ_g and viscosities μ , μ_g , respectively. The problem will initially be formulated for the case in which the ambient fluid is a gas, hence the subscripts ‘g’, but we will later see that, under certain simplifying assumptions, this formulation is equivalent to the case in which the ambient fluid is a second immiscible liquid.

The problem has an axial symmetry and symmetry with respect to the plane tangential to the drops at the moment of their initial contact, so that it is sufficient

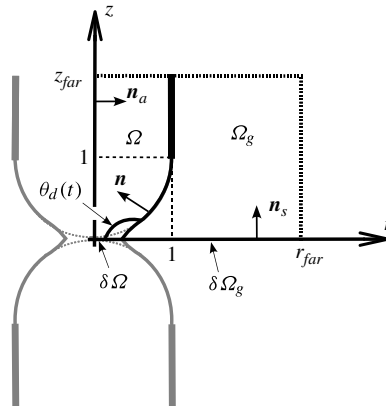


FIGURE 2. Sketch indicating aspects of the problem formulation for the coalescence of two identical hemispheres grown from syringes.

and convenient to consider the flow only in the first quadrant of the (r, z) plane of the suitably chosen cylindrical coordinate system (figure 2) and use the appropriate symmetry conditions on the axis and the plane of symmetry. Using the initial radius of the drops R as the characteristic length scale, $U_v = \sigma_{1e}/\mu$ (where σ_{1e} is the equilibrium surface tension of the fluid–liquid interface) as the scale for velocities, $T_v = R/U_v = \mu R/\sigma_{1e}$ as the time scale, and σ_{1e}/R as the scale for pressure, we have that the (dimensionless) bulk velocities \mathbf{u}, \mathbf{u}_g and pressures p, p_g in the liquid and the ambient fluid satisfy the Navier–Stokes equations, which in the dimensionless form are given by

$$\nabla \cdot \mathbf{u} = 0, \quad Re \left[\frac{\partial \mathbf{u}}{\partial t} + \mathbf{u} \cdot \nabla \mathbf{u} \right] = \nabla \cdot \mathbf{P}, \quad \mathbf{P} = -p\mathbf{I} + [\nabla \mathbf{u} + (\nabla \mathbf{u})^T], \quad \mathbf{r} \in \Omega, \tag{2.1a-c}$$

$$\nabla \cdot \mathbf{u}_g = 0, \quad \bar{\rho} Re \left[\frac{\partial \mathbf{u}_g}{\partial t} + \mathbf{u}_g \cdot \nabla \mathbf{u}_g \right] = \nabla \cdot \mathbf{P}_g, \quad \mathbf{P}_g = -p_g\mathbf{I} + \bar{\mu}[\nabla \mathbf{u}_g + (\nabla \mathbf{u}_g)^T], \quad \mathbf{r} \in \Omega_g. \tag{2.2a-c}$$

Here t is time; \mathbf{P} and \mathbf{P}_g are the stress tensors in the liquid and the fluid, respectively; \mathbf{I} is the metric tensor of the coordinate system; and Ω and Ω_g indicate the regions occupied by the liquid and the ambient fluid (figure 2). The non-dimensional parameters are the Reynolds number $Re = \rho\sigma_{1e}R/\mu^2$ based on the liquid’s properties, the fluid-to-liquid density ratio $\bar{\rho} = \rho_g/\rho$ and the corresponding viscosity ratio $\bar{\mu} = \mu_g/\mu$.

The interface formation model (Shikhmurzaev 2007), which we will be using to formulate the boundary conditions, states that part of the free surface trapped between the drops ($\partial\Omega$ in figure 2) does not lose its specific surface properties, such as the surface tension, instantly, so that, until it does, one will have a gradually disappearing ‘internal interface’ whose (residual) surface tension can sustain an angle in the free surface (figure 1). Pictorially, one has a process analogous to dynamic wetting where the drops ‘spread’ over the separating plane of symmetry, with the ‘contact line’ at $r = r_c(t)$, $z = 0$ leaving behind a gradually disappearing interface. Using this analogy, the point in the (r, z) plane at which the free surface of the upper drop

meets the plane of symmetry will be referred to as the ‘contact line’ and the angle θ_d between this free surface and the symmetry plane $z=0$ will be called the ‘contact angle’. As the contact angle reaches its ‘equilibrium value’ of 90° , the free surface becomes smooth and the conventional model takes over as the interface formation model simply reduces to it.

Both the free surface and the internal interface will be described as two-dimensional ‘surface phases’ characterized by their surface tensions σ_i , surface densities ρ_i^s and surface velocities \mathbf{v}_i^s , where $i = 1, 2$, with subscripts 1 and 2 hereafter labelling the surface parameters of the free surface and the internal interface, respectively. We will scale the surface velocities with U_v , the surface tensions with σ_{1e} and the surface densities with a characteristic surface density $\rho_{(0)}^s$.

On the free surface, besides the standard normal and tangential stress boundary conditions,

$$\mathbf{n} \cdot (\mathbf{P} - \mathbf{P}_g) \cdot \mathbf{n} = \sigma_1 \nabla \cdot \mathbf{n}, \tag{2.3}$$

$$\mathbf{n} \cdot (\mathbf{P} - \mathbf{P}_g) \cdot (\mathbf{I} - \mathbf{nn}) + \nabla \sigma_1 = 0, \tag{2.4}$$

where \mathbf{n} is a unit normal pointing into the liquid, one has (a) the kinematic condition

$$\frac{\partial f}{\partial t} + \mathbf{v}_1^s \cdot \nabla f = 0, \tag{2.5}$$

where $f(r, z, t) = 0$, with the *a priori* unknown function f , describes the evolution of the free-surface shape and \mathbf{v}_1^s is the corresponding velocity, (b) the surface equation of state, which in both interfaces will be taken in the simplest linear form

$$\sigma_i = \lambda(1 - \rho_i^s) \quad (i = 1, 2), \tag{2.6}$$

where λ is a constant and ρ_i^s is the dimensionless surface density, (c) the surface continuity equation incorporating the mass exchange between the bulk and surface phases, and the corresponding equation for the normal component of the bulk velocity,

$$\epsilon \left[\frac{\partial \rho_1^s}{\partial t} + \nabla \cdot (\rho_1^s \mathbf{v}_1^s) \right] = -(\rho_1^s - \rho_{1e}^s), \quad (\mathbf{u} - \mathbf{v}_1^s) \cdot \mathbf{n} = Q(\rho_1^s - \rho_{1e}^s), \tag{2.7a,b}$$

where ϵ , ρ_{1e}^s and Q are constants, (d) the kinematic condition for the normal component of the ambient fluid velocity,

$$(\mathbf{u}_g - \mathbf{v}_1^s) \cdot \mathbf{n} = 0, \tag{2.8}$$

and (e) equations relating the tangential components of the bulk velocities and stresses on the two sides of the interface, the surface velocity and the gradients of surface tension,

$$\frac{1}{2} \bar{\alpha} \mathbf{n} \cdot (\mathbf{P} + \mathbf{P}_g) \cdot (\mathbf{I} - \mathbf{nn}) = A(\mathbf{u} - \mathbf{u}_g) \cdot (\mathbf{I} - \mathbf{nn}), \tag{2.9}$$

$$[\mathbf{v}_1^s - \frac{1}{2}(\mathbf{u} + \mathbf{u}_g) - \bar{\alpha} \nabla \sigma_1] \cdot (\mathbf{I} - \mathbf{nn}) = 0, \tag{2.10}$$

where $\bar{\alpha}$ and A are constants. The constant $\bar{\beta}$, which has been introduced in previous works (Shikhmurzaev 2007), is $\bar{\beta} = A\bar{\alpha}^{-1}$. The non-dimensional constants appearing in (2.5)–(2.10) incorporate the corresponding material constants whose physical meanings and values for some systems are described elsewhere (see Shikhmurzaev 2007).

The location of the internal interface is known, $z = 0$, and hence $\mathbf{v}_2^s \cdot \mathbf{n}_s = 0$, where \mathbf{n}_s is a unit normal to the plane of symmetry (figure 2). Then, on this interface one has only the tangential stress condition

$$\mathbf{n}_s \cdot \mathbf{P} \cdot (\mathbf{I} - \mathbf{n}_s \mathbf{n}_s) + \nabla \sigma_2 = 0, \tag{2.11}$$

analogous to (2.4); the surface continuity equation together with the corresponding condition on the normal component of the bulk velocity,

$$\epsilon \left[\frac{\partial \rho_2^s}{\partial t} + \nabla \cdot (\rho_2^s \mathbf{v}_2^s) \right] = -(\rho_2^s - 1), \quad \mathbf{u} \cdot \mathbf{n}_s = Q(\rho_2^s - \rho_{2c}^s), \tag{2.12a,b}$$

analogous to (2.7); and the equation

$$[4A(\mathbf{v}_2^s - \mathbf{u}) - \bar{\alpha}(1 + 4A)\nabla \sigma_2] \cdot (\mathbf{I} - \mathbf{n}_s \mathbf{n}_s) = 0, \tag{2.13}$$

which relates the difference between the tangential components of the surface and bulk velocity to the surface tension gradient in the surface phase.

At the moving ‘contact line’, $r = r_c(t)$, $z = 0$, we have the conditions of continuity of the surface mass flux and the force balance in the projection on the symmetry plane,

$$\rho_1^s(\mathbf{v}_1^s - \mathbf{U}_c) \cdot \mathbf{m}_1 + \rho_2^s(\mathbf{v}_2^s - \mathbf{U}_c) \cdot \mathbf{m}_2 = 0, \tag{2.14}$$

$$\sigma_2 + \sigma_1 \cos \theta_d = 0, \tag{2.15}$$

where $\mathbf{U}_c = d\mathbf{r}_c/dt$; the unit vectors \mathbf{m}_i are normal to the contact line and inwardly tangential to the free surface ($i = 1$) and the plane of symmetry ($i = 2$); and θ_d is the ‘contact angle’ (figure 2). Equation (2.15) is analogous to the well-known Young’s equation (Young 1805) that introduces and determines the contact angle in the process of dynamic wetting. Notably, the surface continuity equation (2.12) together with (2.6) and (2.15) ensure that the completion of the coalescence process associated with the internal interface reaching its equilibrium state ($\rho_2^s = 1$) results in the disappearance of this interface ($\sigma_2 = 0$) and the restoration of the familiar smooth free surface ($\theta_d = 90^\circ$), thus allowing the conventional model to take over.

For the ambient fluid phase, on the plane of symmetry $z = 0$ one has conditions of impermeability and zero tangential stress,

$$\mathbf{u}_g \cdot \mathbf{n}_s = 0, \quad \mathbf{n}_s \cdot \mathbf{P}_g \cdot (\mathbf{I} - \mathbf{n}_s \mathbf{n}_s) = 0 \quad (\mathbf{r} \in \partial\Omega_g), \tag{2.16a,b}$$

and, for the liquid phase, at the axis of symmetry $r = 0$ one has the appropriate symmetry conditions,

$$\mathbf{u} \cdot \mathbf{n}_a = 0, \quad \frac{\partial}{\partial r} [\mathbf{u} \cdot (\mathbf{I} - \mathbf{n}_a \mathbf{n}_a)] = 0, \quad \mathbf{v}_2^s \cdot \mathbf{n}_a = 0, \tag{2.17a,b}$$

where \mathbf{n}_a is a unit normal to the axis of symmetry in the (r, z) plane. At the point in the (r, z) plane where the (initially hemispherical) free surface meets the syringe tip we have a pinned contact line:

$$f(1, 1, t) = 0 \quad (t \geq 0). \tag{2.18}$$

It is assumed that, in the far field, the exterior fluid and the liquid inside the syringe are at rest, whilst on the cylinder’s surface, the no-slip condition is applied to both phases, so that

$$\mathbf{u}, \mathbf{u}_g \rightarrow \mathbf{0} \quad \text{as } r^2 + z^2 \rightarrow \infty, \quad \mathbf{u} = \mathbf{u}_g = \mathbf{0} \quad \text{at } r = 1, \quad z \geq 1. \tag{2.19a,b}$$

As the initial conditions, we set that both the liquid and the fluid are at rest, the free surface is in equilibrium,

$$\mathbf{u} = \mathbf{u}_g = \mathbf{0}, \quad \rho_1^s = \rho_{1e}^s \quad (t = 0), \quad (2.20a,b)$$

and the free surface has the shape of a hemisphere,

$$f(r, z, 0) = r^2 + (z - 1)^2 - 1 = 0. \quad (2.21)$$

For computations using the conventional model, the formulation described above can still be used if the parameter ϵ is set to zero so that the interface formation dynamics is ‘turned off’.

3. Computational details

In order to solve the problem, we employ the finite-element-based computational platform described in Sprittles & Shikhmurzaev (2012c, 2013), where one can find a user-friendly step-by-step algorithm for its implementation (see appendix A of the present paper for a small correction to Sprittles & Shikhmurzaev 2013). In the present work, we only need (a) to extend it to incorporate the dynamics of the ambient fluid, which can be done in a straightforward way, and (b) to adjust the problem formulation described above for the numerical treatment. The latter means, firstly, truncating the computational domain by introducing the ‘far-field’ boundary at a large but finite distance from the origin. This far-field boundary is shown schematically in figure 2, where r_{far} and z_{far} have to be sufficiently far away from the origin for their location and the soft boundary conditions we impose there to have a negligible effect on the coalescence dynamics.

The second adjustment that we have to make is to introduce a small but finite radius r_{min} of the initial contact of the two drops, so that initially we have the internal interface at $0 < r < r_{min}$, $z = 0$, where we will use the initial condition

$$\rho_2^s = \rho_{1e}^s, \quad (3.1)$$

stating that the trapped part of the free surface has not yet started relaxing towards its eventual equilibrium state of $\rho_2^s = 1$ (at which point the surface has no tension $\sigma_2 = 0$). As the initial shape of the free surface, we will take simply a truncated sphere or hemisphere satisfying $z(r_{min}) = 0$,

$$(r - r_{min})^2 + (z - z_0)^2 = z_0^2, \quad (3.2)$$

where $z_0 = [1 + (1 - r_{min})^2]/2$, so that, if there is no base, i.e. $r_{min} = 0$, one has $z_0 = 1$ and hence $r^2 + (z - 1)^2 = 1$, thus recovering (2.21).

If the conventional model is used, as described in detail in Sprittles & Shikhmurzaev (2012a), the initial free-surface shape is taken from the analytic solution in Hopper (1984), obtained for Stokes flow, to be

$$r(\theta) = \sqrt{2}\{(1 - m^2)(1 + m^2)^{-1/2}[1 + 2m \cos(2\theta) + m^2]^{-1}\}(1 + m) \cos \theta, \quad (3.3)$$

$$z(\theta) = \sqrt{2}\{(1 - m^2)(1 + m^2)^{-1/2}[1 + 2m \cos(2\theta) + m^2]^{-1}\}(1 - m) \sin \theta, \quad (3.4)$$

for $0 < \theta < \theta_u$, where m is chosen such that $r(0) = r_{min}$ is the initial bridge radius, which we choose, and θ_u is chosen such that $r(\theta_u) = z(\theta_u) = 1$. Notably, for $r_{min} \rightarrow 0$

we have $m \rightarrow 1$ and $r^2 + (z - 1)^2 = 1$, i.e. the drop's profile is a semicircle of unit radius that touches the plane of symmetry at the origin as required.

Importantly, unlike the conventional model, for the interface formation model the limit $r_{min} \rightarrow 0$ does not give rise to a singularity (Shikhmurzaev 2007), so that here a non-zero value of r_{min} is used for convenience of the computations and no special shape is required to artificially enforce smoothness of the free surface. We will look at how the value of r_{min} influences the outcome of computations in § 5.1.

4. Simplifications for $Q, \bar{\alpha} \rightarrow 0$ with $A = O(1)$

For the case of an inviscid dynamically passive ambient fluid, the full model, set out in § 2, has been studied in Sprittles & Shikhmurzaev (2012a). The results of this study suggest an asymptotic simplification that facilitates the computations. Before extending the earlier work to include the full dynamics of the viscous ambient gas or liquid, we take the limit $\bar{\alpha} \rightarrow 0$ with $A = O(1)$. As shown by experiments (Shikhmurzaev 1996; Blake & Shikhmurzaev 2002), $\alpha \sim \mu^{-1}$ and, given that $\bar{\alpha} = \alpha\mu/R$, for the class of liquids considered in the present work, $\alpha\mu \approx 10^{-9}$ m (Blake & Shikhmurzaev 2002), so that $\bar{\alpha} = 10^{-9}$ (m)/ R (m) and, for drops that are larger than a micrometre, $R > 10^{-6}$ m, we have $\bar{\alpha} < 10^{-3} \ll 1$. Importantly, unlike the case of dynamic wetting (Shikhmurzaev 2007), the solution to the coalescence problem remains singularity-free in the limit $\bar{\alpha} \rightarrow 0$, $A = O(1)$, so that, to leading order, we can simply set $\bar{\alpha} = 0$ in the above formulation.

The computations in the framework of the simplified system have been compared to results for the full system of equations as computed in Sprittles & Shikhmurzaev (2012a). In the range of parameters considered in Sprittles & Shikhmurzaev (2012a), and therefore those considered here, curves for all the relevant quantities proved to be very close for the two systems and, consequently, henceforth the simpler system will be used. It is important to note, however, that as much smaller scales are approached, such a simplification may no longer be valid.

The essence of what this asymptotic limit is about is very simple. From (2.9) and (2.10), it can be seen that, in this limit, the differences between the components of velocity tangential to the free surface on either side of the surface as well as between these components and the surface velocity itself become negligible, $\mathbf{u}_{||} = \mathbf{u}_{g||} = \mathbf{v}_{1||}^s$. (Here subscript || denotes the component of a vector tangential to a surface, i.e. it represents the convolution of the vector with the tensor $(I - \mathbf{nn})$ which extracts the tangential components of vectors and tensors.) In other words, in this limit we recover the classical condition of continuity of the tangential component of velocity across an interface. Similarly, on the internal interface, from (2.13), we have that $\mathbf{u}_{||} = \mathbf{v}_{2||}^s$. Basically, the limit $\bar{\alpha} \rightarrow 0$, $A = O(1)$ in our system of equations leads to the transport of surface mass along the interfaces being due to the bulk velocity tangential to that interface, rather than to surface tension gradients acting inside the interface, i.e. to the situation one has in the classical fluid mechanics model.

When extending this approach from an inviscid dynamically passive gas to the case of a viscous gas, as with the conventional model, the effect of the gas now manifests itself only through the balance of stress terms (2.3) and (2.4), with \mathbf{P}_g composed of a dynamic pressure and non-zero viscous terms.

A further simplification is also to consider $Q \rightarrow 0$ in (2.7), that is, to assume that the flux of mass into or out of the interface affects only the surface dynamics, rather than the bulk flow also. In other words, as in the classical case, the normal velocity is also now continuous across an interface so that on the free surface $\mathbf{u} \cdot \mathbf{n} = \mathbf{u}_g \cdot \mathbf{n} = \mathbf{v}_1^s \cdot \mathbf{n}$

and at the plane of symmetry $\mathbf{u} \cdot \mathbf{n}_s = \mathbf{v}_2^s \cdot \mathbf{n}_s = 0$. Given that $Q = \rho_{(0)}^s / (\rho \sigma \tau_\mu)$, estimates suggest that $Q \sim 10^{-2} \ll 1$ for the liquids considered, so that the effect of taking $Q = 0$ is also negligible. Simulations with a finite Q have confirmed this. As a result, one has the conventional formulation used for capillary flows in which the surface tension on an interface is considered dynamic combined with an equation of state (2.6) and the surface continuity equation,

$$\epsilon \left[\frac{\partial \rho_i^s}{\partial t} + \nabla \cdot (\rho_i^s \mathbf{u}) \right] = -(\rho_i^s - \rho_{ie}^s), \quad i = 1, 2, \quad (4.1)$$

where $\rho_{2e}^s = 1$. As the single surface equation only contains first-order derivatives in space, (2.14) is no longer applicable and a single boundary condition is applied on the surface density where each interface meets the axis of symmetry or the syringe tip. In contrast with the case of dynamic wetting, where the motion of the contact line relative to the solid forces the mass flux through the contact line, in the case of coalescence the contact line moves as if to minimize the stress in its vicinity and does so by becoming a stagnation line for the bulk flow (in the reference frame moving with the contact line). As a result, condition (2.14) appears to be satisfied with both terms on the left-hand side equal to zero.

In taking the aforementioned simplifications, the interface formation model is stripped down to its simplest form which has the advantage that (a) there are fewer free parameters that have to be estimated and (b) it becomes easier to isolate the key features of the interface formation model that distinguish it from the conventional model's predictions. A notable consequence of the simplified formulation is that the ambient fluid can be either a viscous gas or an immiscible liquid, in contrast to the case of $Q \neq 0$ where a second liquid would mean that the mass exchange on both sides of the interface would have to be considered (Shikhmurzaev 2007).

5. Parametric study of the model

To establish an appropriate parameter range, and to compare to experimental data from Paulsen *et al.* (2011) in §6, consider the parameter values based on water-glycerol drops, and initially take them to have $R = 2$ mm radii. These mixtures have the advantage that their surface tension with air $\sigma = 65$ mN m⁻¹ and density $\rho = 1200$ kg m⁻³ remain approximately constant, whilst the viscosity can range over three orders of magnitude $\mu = 10^{-3}$ –1 Pa s. Then the Reynolds number is in the range $Re = 10^{-1}$ – 10^5 . For coalescence in air of density $\rho_g = 1.2$ kg m⁻³ and viscosity $\mu_g = 18$ μ Pa s, the gas-to-liquid density ratio is $\bar{\rho} = 10^{-3}$ throughout and the viscosity ratio will be in the range $\bar{\mu} = 10^{-5}$ – 10^{-2} .

Since our problem is both nonlinear and multi-parametric, a sensible strategy for exploring it would be to use the estimates for the material constants of the interface formation model obtained from experiments on dynamic wetting (Blake & Shikhmurzaev 2002), where the model was used without any alterations, as a 'base case' and to investigate how a variation of these parameters influences the model's predictions. The experimental results in Blake & Shikhmurzaev (2002) suggest that for the class of fluids considered, i.e. water-glycerol mixtures, the relaxation time of the interface $\tau = \tau_\mu \mu$, where τ_μ is approximately constant across all the mixtures considered, so that the dimensionless parameters are $\epsilon = \sigma \tau_\mu / R$, $\rho_{1e}^s = (\rho_{1e}^s)_{dim} / \rho_{(0)}^s$ and $\lambda = \gamma \rho_{(0)}^s / \sigma_{1e}$. Using previous estimates for these parameters as our base state

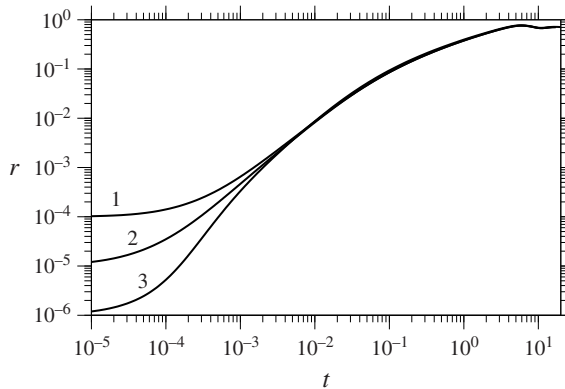


FIGURE 3. Effect of decreasing initial bridge radius for the base case ($Re_0 = 68$ and $\bar{\mu}_0 = 4 \times 10^{-4}$) with: 1, $r_{min} = 10^{-4}$; 2, $r_{min} = 10^{-5}$; and 3, $r_{min} = 10^{-6}$. As expected, the value of r_{min} becomes insignificant shortly after the start of the process.

(denoted with a subscript ‘0’), about which the parameters can be varied to identify their role, we have

$$\epsilon_0 = 3.3 \times 10^{-5}, \quad (\rho_{1e}^s)_0 = 0.4, \quad \lambda_0 = (1 - \rho_{1e}^s)^{-1}, \quad (5.1a-c)$$

where $\tau_\mu = 10^{-6} \text{ m}^2 \text{ N}^{-1}$, consistent with previous estimates in Blake & Shikmurzaev (2002), so that the relaxation time for a viscosity of $\mu = 10^{-3} \text{ Pa s}$ (water) is 1 ns whilst for $\mu = 1 \text{ Pa s}$ (roughly, pure glycerol) it is $\tau = 1 \text{ }\mu\text{s}$. In our comparison to experiment in § 6, values from (5.1) will be used across all liquids, in contrast to Sprittles & Shikmurzaev (2012a) where ρ_{1e}^s was fitted. At present, no study has been conducted on the influence of this parameter on the mixture’s properties, so, again, the simplest possibility is considered.

In order to further our understanding of the mechanisms governing the interface formation/disappearance process, we will look into how varying these parameters around their base state influences the propagation of the liquid bridge connecting the coalescing drops for the intermediate viscosity of $\mu = 48 \text{ mPa s}$, so that $Re_0 = 68$ and $\bar{\mu}_0 = 4 \times 10^{-4}$.

5.1. Influence of initial conditions

Before considering the effect of the interface formation parameters on the coalescence event, we would like to establish the effect that our initial conditions, in particular the finite bridge radius r_{min} at which the computations are started, have on the subsequent dynamics. In figure 3 the effect of the initial radius r_{min} in (3.2) is shown, and it can be seen that after a certain time, or distance, all the curves fall on top of each other. Specifically, one can see that after around $r = 10r_{min}$ the effect of the initial conditions has diminished and the curves begin to fall onto a single line. A similar result has been obtained for the conventional model. Thus, henceforth, computational results will be shown from $r = 10r_{min}$ so that the range under consideration has not been affected by the finite initial radius, i.e. the same curve would be obtained for smaller r_{min} . This reinforces the point that it is not the amount of trapped interface that is initially formed that matters, but the subsequent dynamics.

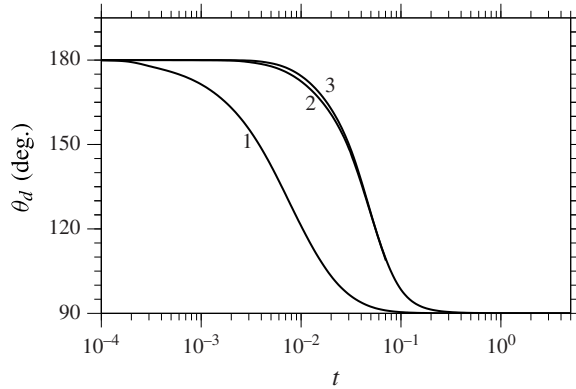


FIGURE 4. Influence of interface formation parameters on the evolution of the contact angle θ_d for $Re_0 = 68$ and $\bar{\mu}_0 = 4 \times 10^{-4}$. Curve 1 is the base case used in previous calculations; curve 2 is for $10\epsilon_0$; and curve 3 is for $\lambda = 10\lambda_0$. The last two curves highlight the existence of three distinct stages of the process: (a) the very initial stage where the drops ‘touch’ with their free surface forming a cusp, (b) the relaxation stage where there is an evolving corner between free surfaces and (c) the ‘equilibrium’ stage when the conventional model takes over.

Notably, although with the interface formation model $r_{min} = 10^{-5}$ can easily be resolved, so that $r > 10^{-4}$ becomes independent of r_{min} , these values cannot be achieved with computations of the conventional model, where the radius of curvature at the bridge front becomes prohibitively small for $r_{min} < 10^{-4}$, owing to the requirement that, in the framework of this model, the bridge must be smooth. As a result, although in the parametric study we look at $r > 10^{-4}$, in order to ensure that both the conventional and interface formation models are treated on an equal footing in our comparison with experiments in § 6, computed curves and experimental results are considered from $r = 10^{-3}$ following a limitation imposed by the conventional model.

5.2. Role of the interface formation parameters

From figure 4, one can see that the stage during which the interface formation dynamics is occurring, i.e. the period in which the free surface is not smooth ($\theta_d \neq 90^\circ$), comprises different regimes. In what we will refer to as the very initial stages, around $t < T_{ini} = 10^{-3}$ for the base state (curve 1), the angle at which the free surface meets the plane of symmetry stays approximately constant, $\theta_d \approx 180^\circ$. This can be seen most clearly in curves 2 and 3. Then one has the ‘relaxation stage’, around $T_{ini} < t < T_{rel} = 10^{-2}$ for the base state, where the angle relaxes to $\theta_d \approx 90^\circ$, after which the interface formation model turns into the conventional one, as can be seen in figure 6.

Figure 5 shows the time dependence of the surface tension at the contact line σ_{cl} on each interface. As we can see, in the very initial stage $\sigma_1 = \sigma_2 = \sigma_{ini}(t)$, evolving from $\sigma_{ini}(t) = 1$ at $t = 0$ imposed by our initial conditions to $\sigma_{ini}(t) \approx 0.6$ at $t = T_{ini} = 10^{-3}$. This is a very interesting feature, as it indicates that both the free surface and the internal interface are being stretched, approximately in equal measure, as the process of coalescence goes through its very initial stage. From the force balance at

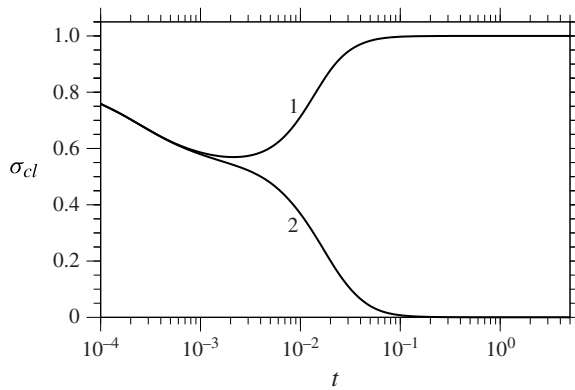


FIGURE 5. Evolution of the surface tension where the free surface meets the plane of symmetry (at the ‘contact line’) on: 1, the free surface; and 2, the internal interface obtained for $Re_0 = 68$ and $\bar{\mu}_0 = 4 \times 10^{-4}$. The very initial stage where the two surface tensions evolve together due to the stretching of both interfaces by the bulk flow is followed by the relaxation stage where they evolve towards their equilibrium values. Once these values are reached, the conventional model takes over.

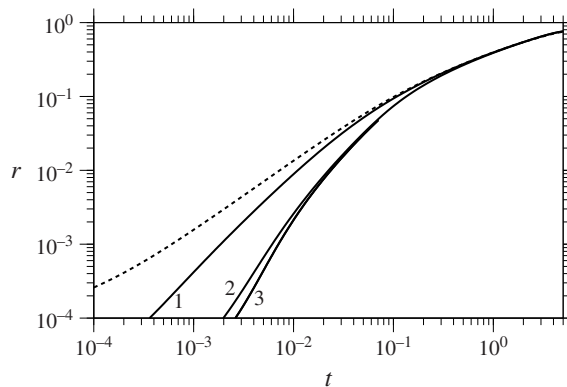


FIGURE 6. Influence of interface formation parameters at $Re_0 = 68$ and $\bar{\mu}_0 = 4 \times 10^{-4}$. Curve 1 is the base case used in previous calculations; curve 2 is for $10\epsilon_0$; and curve 3 is for $\lambda = 10\lambda_0$. The dashed line is the conventional model’s prediction.

the contact line (2.15), $\sigma_1 = \sigma_2$ leads immediately to $\theta_d = 180^\circ$, as already noted from figure 4.

At time $t = T_{ini}$, the relaxation stage takes over, during which the liquid–fluid and internal interface approach their equilibrium states of $\sigma_1 = 1$ and $\sigma_2 = 0$ at $t = T_{rel}$. For the liquid–fluid interface, which started in equilibrium but was then driven out of this state by the coalescence process, this relaxation stage involves an increase in surface tension, whilst for the internal interface, the surface tension continues to decrease until it reaches a state where this interface has effectively ‘disappeared’ and no longer has surface properties that would distinguish it from the bulk phase. In other words, the process of coalescence as modelled by the interface formation model is complete when $t = T_{rel}$. Given that the process naturally divides into these different stages, we now consider the effect of the interfacial parameters in each, as illustrated in figure 6.

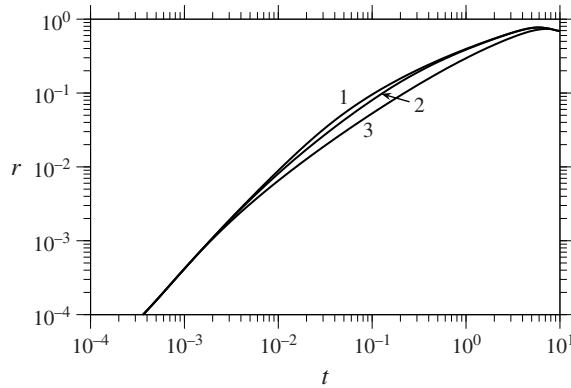


FIGURE 7. Effect of the viscosity ratio on bridge propagation, with all other parameters set to their base values: 1, $\bar{\mu} = 10^{-4}$; 2, $\bar{\mu} = 10^{-2}$; and 3, $\bar{\mu} = 1$. Strikingly, although the gap between the free surfaces is narrowest in the very initial stage of the process, the ambient fluid-to-liquid viscosity ratio has no effect there.

The two parameters that we vary, ϵ and $\lambda = 1/(1 - \rho_{1e}^s)$, can be seen from figure 4 to affect the time during which $\theta_d \approx 180^\circ$, i.e. the time scale of the very initial stages $t < T_{ini}$. Roughly, a factor of 10 increase in either ϵ (curve 2) or λ (curve 3) is seen to increase the time of the very initial stage by a factor of 10. From figure 6, we can see that the longer the coalescence process spends in this initial stage, the slower the initial motion.

The two controlling parameters are seen to have a similar effect on the relaxation stage, with this period extending by a factor of 10 to $T_{rel} \approx 10^{-1}$, as opposed to $T_{rel} \approx 10^{-2}$ for the base case, when either ϵ or λ are increased by a factor of 10. Figure 6 confirms what one may expect, that the earlier the interface formation process is over, the faster the bridge speed propagation will be. This is to be expected, as in the limit $T_{rel} \rightarrow 0$, in which $\theta_d = 90^\circ$ in an infinitesimal time, we have the dynamics of the conventional model, which is known to have a singular velocity at the start of the process, so that larger T_{rel} must give a slower coalescence speed. Notably, we see that, for $t > 0.1$, all the curves coincide, as the conventional model takes over so that the interfacial parameters no longer have an influence on the dynamics.

5.3. Influence of the ambient fluid

To consider the influence of the ambient fluid on the coalescence process, all the base parameters remain fixed with the exception of $\bar{\mu}$ and $\bar{\rho}$, which are now allowed to vary. For $\bar{\rho} \leq 0.01$, corresponding to the range of realistic liquid–gas systems, which are our main focus here, the influence of the finite gas density on the dynamics of coalescence is seen to be negligible so that, henceforth, we will consider only the effect of the viscosity ratio $\bar{\mu}$.

In figure 7, the effect of the viscosity ratio on the bridge propagation is shown, and what is immediately striking is that for $r < 10^{-2}$ an increase of two orders of magnitude in viscosity ratio, from $\bar{\mu} = 10^{-4}$ (curve 1) to $\bar{\mu} = 10^{-2}$ (curve 2), has little effect on the speed of coalescence. Similarly, increasing by four orders of magnitude to $\bar{\mu} = 1$ does not alter the bridge evolution for $r < 10^{-3}$. Only after a finite time does the initial indifference to $\bar{\mu}$ give way to an effect of viscosity ratio: as one would expect, larger viscosity ratios result in a slower speed of coalescence. Comparing

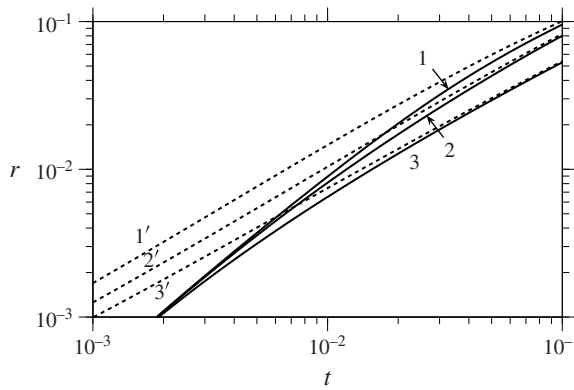


FIGURE 8. Effect of the viscosity ratio on bridge propagation for the two different models, with all other parameters set to their base values: 1, $\bar{\mu} = 10^{-4}$; 2, $\bar{\mu} = 10^{-2}$; 3, $\bar{\mu} = 1$. The predictions of the conventional model are shown by dashed lines, with curve numbers labelled with a prime.

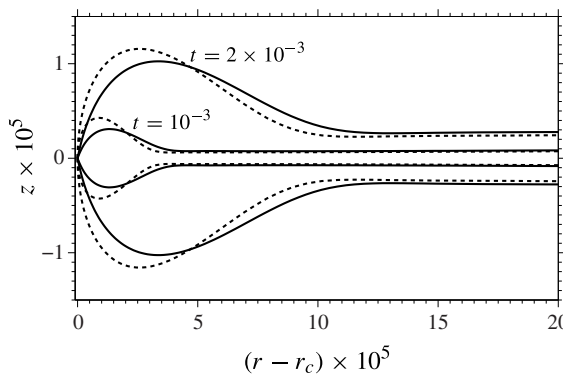


FIGURE 9. Free-surface shapes obtained from the interface formation model (solid lines) and the conventional model (dashed lines) at $t = 10^{-3}$ and $t = 2 \times 10^{-3}$.

$\bar{\mu} = 10^{-4}$ (curve 1) and $\bar{\mu} = 10^{-2}$ (curve 2), it can be seen that only in the period $10^{-2} < r < 10^{-1}$ is there a noticeable difference caused by the change in $\bar{\mu}$.

Figure 8 shows that the behaviour observed for the interface formation model (solid lines) differs significantly from that computed for the conventional model (dashed lines). In the conventional model, the effect of the viscosity ratio is instantaneously felt and the deviation caused by the differences in $\bar{\mu}$ remains roughly constant (on a log-log plot) for $r < 0.1$. In contrast, for the interface formation model, only after a finite time do the curves fan out, with the distance between them increasing whilst $r < 0.1$.

In an attempt to understand the observed behaviour, in figure 9, the free-surface shape of the bridge front is shown at two instants in time, $t = 10^{-3}$ and 2×10^{-3} , for the two different models. It can be seen that, for the interface formation model at $t = 10^{-3}$, the free surface is not smooth, and compared to the conventional model's shape at this time there is less of a 'bubble' of fluid trapped in front of the bridge. It could be that it is this geometrical feature, present only in the interface formation dynamics,

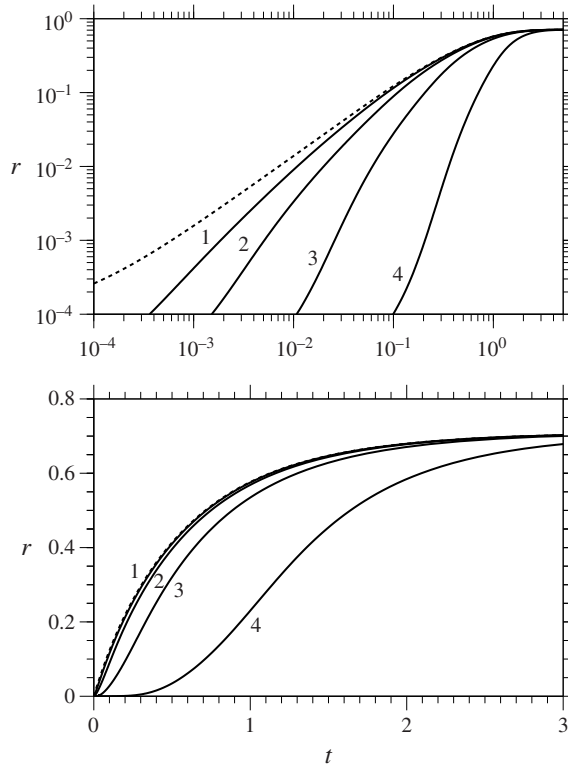


FIGURE 10. Effect of decreasing the radius of the drops on the bridge propagation (plotted in two different ways) with: 1, $R = 2$ mm; 2, $R = 200$ μm ; 3, $R = 20$ μm ; and 4, $R = 2$ μm . The dashed line is the computed solution for the conventional model, which for the $Re = 0$ case considered here is independent of drop size.

which results in the ambient fluid having less of an effect for this model than for the conventional model where the free surface is always smooth (dashed lines). In other words, as the process enters the relaxation stage and the angle evolves from $\theta_d = 180^\circ$ to $\theta_d = 90^\circ$, ambient fluid is more easily swept away from the bridge front region and thus has little effect on the dynamics. In contrast, in the conventional model, a bubble of fluid builds up in front of the bridge front, so that its dynamics and removal become necessary for the bridge to propagate and thus its behaviour, governed by the value of $\bar{\mu}$, alters the speed of coalescence. For the interface formation model, once the free surface becomes smooth and matters are handed over to the conventional one, similar effects are observed.

5.4. Effect of drop size

Consider how the speed of coalescence depends on the size of the drop R . To further simplify matters, consider the usual base case except for $Re = 0$, i.e. a high-viscosity solution. In this case, there is a universal curve describing the bridge propagation for the conventional model; this curve is shown as a dashed line in figure 10. However, for the interface formation model, the parameter $\epsilon = \sigma\tau_\mu/R = 6.5 \times 10^{-8} R^{-1}$ depends on the size of the drop. Therefore, the conventional model predicts no change in the curve relating (dimensionless) bridge radius r to (dimensionless) time t , whilst the

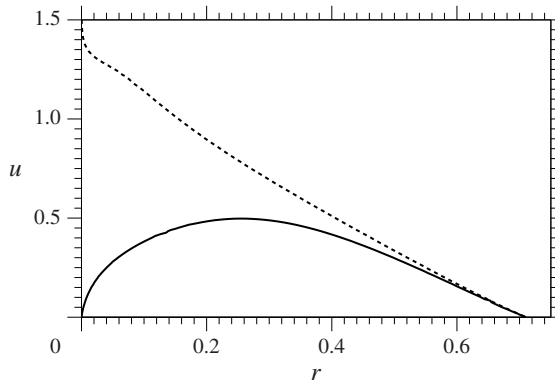


FIGURE 11. Bridge speed u as a function of bridge radius for $R = 2 \mu\text{m}$, with the solid line corresponding to the interface formation model's predictions and the dashed line the conventional model's.

interface formation model could predict some effect, and it is this which will now be quantified.

In figure 10, the bridge evolution is shown on both log–log and linear plots. From an experimental perspective it is likely that the linear plot will prove more useful, so it is this we shall focus on. What can be seen is that, although differences can be observed on the log–log plot for larger drops $R > 200 \mu\text{m}$ (curves 1, 2), deviations from the conventional model's predictions (dashed line) are relatively small on the linear one. However, for $R = 20 \mu\text{m}$ (curve 3) a noticeable deviation from the conventional model's universal curve is observed, and for $R = 2 \mu\text{m}$ a huge change is seen with the coalescence speed dramatically reduced.

The changes for small drops are most easily seen in figure 11, where the bridge speed for the smallest drops considered ($R = 2 \mu\text{m}$) is plotted as a function of the bridge's radius. The conventional model's universal solution predicts a monotonically decreasing speed throughout the coalescence process, whilst the interface formation model predicts a clear maximum around $r = 0.25$. From an experimental perspective, it may be easier to observe this maximum in the bridge speed for small drops, rather than trying to compare the bridge evolution across different sized drops as shown in figure 10.

Figure 11 highlights the key difference between the two models' predictions: the conventional model is singular, whilst the interface formation model is singularity-free. Specifically, in the case of the interface formation model, in figure 11 we can see that the initial speed of coalescence is very small, and only over a finite and relatively large time does the bridge front accelerate to a maximum, before relaxing towards its equilibrium (static) shape. In contrast, the initial speed for the conventional model is singularly large and it can only go down as free-surface curvature and hence the capillary pressure that drives the pressure decreases. Although such features are present in all calculations, it is only when the drop's size becomes comparable to the scales on which the interface formation physics acts that these effects visibly change the global motion of the drops.

6. Comparison with experiments

As our base parameters have been set up in order to align with the experiments in Paulsen *et al.* (2011), all that is required here is to specify the viscosity of the

particular mixtures we will consider, which are chosen to give the widest possible range of parameters, and these are $\mu = 3.3, 48, 230$ mPa s. Then, the Reynolds numbers are $Re = 1.4 \times 10^4, 68, 2.9$, and for coalescence in air of density $\rho_g = 1.2 \text{ kg m}^{-3}$ and viscosity $\mu_g = 18 \text{ } \mu\text{Pa s}$, the gas-to-liquid density ratio is $\bar{\rho} = 10^{-3}$ and the viscosity ratios are, respectively, $\bar{\mu} = 5.5 \times 10^{-3}, 3.8 \times 10^{-4}, 7.8 \times 10^{-5}$.

At this stage, we could look to fit our two parameters for the interface formation model to the experimental data. In particular, in Sprittles & Shikhmurzaev (2012a) better agreement between theoretical predictions and experiments was obtained by varying ρ_{1e}^s as a function of fluid viscosity. It is perfectly reasonable for such a variation to occur as the nature of the interface changes with the percentage of glycerol in the mixture; however, here we continue our approach of considering only the simplest possible model and thus use the same parameters across all viscosities.

In figure 12, curves obtained from both the conventional model (curves 1) and the interface formation model (curves 2) are shown for both the case in which the surrounding air is considered viscous and for the situation where the gas is assumed passive (dashed curves marked with a prime). It is apparent that in all cases the viscosity of the gas influences the conventional model's curves, whilst it is only at the lowest viscosity that the gas has a noticeable effect on the interface formation model's predictions. This is consistent with our findings in § 5.3, where we saw that for computations with the interface formation model there is only a small window during which the gas can have an effect on the coalescence speed, which only occurs here at the lowest liquid viscosity, whereas in the conventional model a finite viscosity always has an effect.

In terms of the actual agreement between the models' predictions and the experiments, the viscous gas does not alter the conclusions reached by Sprittles & Shikhmurzaev (2012a): the interface formation model gives a better description of the initial stages of coalescence across two orders of magnitude change in liquid viscosity than the conventional model, whilst for low-viscosity mixtures both models deviate from the experimental measurements of the later stages of coalescence. The possibility that this discrepancy between theory and experiments is caused by the effects of gravity, interface formation and/or the ambient fluid have all been ruled out, suggesting progress in uncovering the reason can only be made by conducting further theory-driven experiments.

7. Discussion

The computational simulations performed have highlighted the role of the ambient fluid's dynamics in the coalescence process and have shown that the effect is different for the two models considered. Despite this, the conclusions from Sprittles & Shikhmurzaev (2012a) remain unchanged. In particular, both the conventional model and the interface formation model, when the latter reduces to the former, give similar predictions for the final stages of the coalescence process, roughly on the millimetre scale, where optical measurements are available. For the flow on the microscale, singularities inherent in the conventional formulation lead to an overprediction of the speed of coalescence. It is only due to the recent experimental results in Paulsen *et al.* (2011) that the errors in the conventional model's predictions could be brought to light. In contrast, the interface formation model is singularity-free in the initial stages and describes the experimental data better, even with the simplifying assumptions used to reduce the number of free parameters.

An analysis of the evolution of the interface formation process sheds light on the time scales involved during a coalescence event. Of particular note is that the time

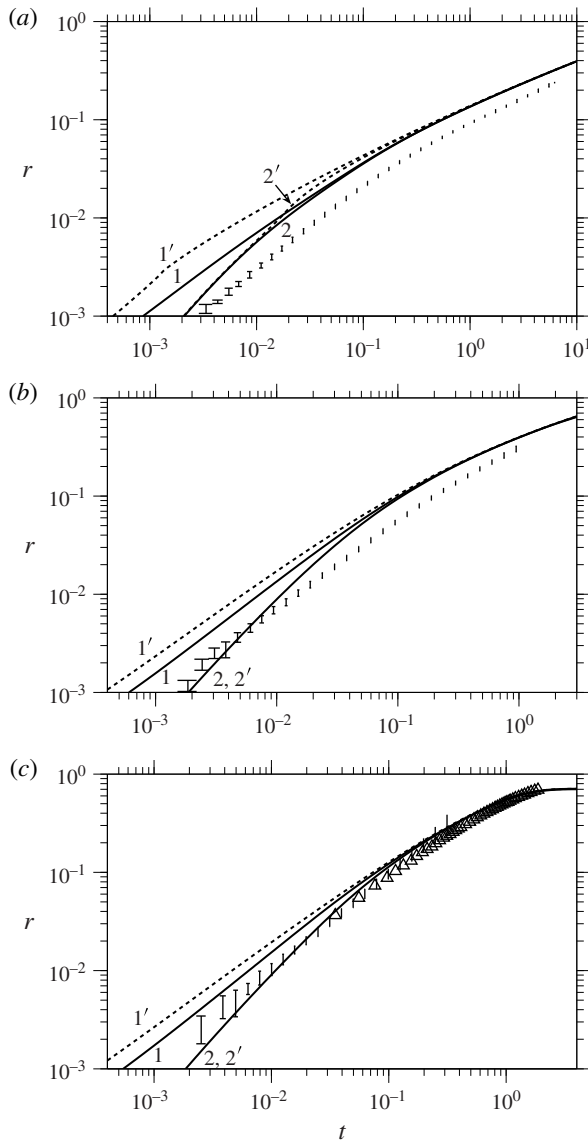


FIGURE 12. Comparison of the predictions of the conventional model (curve 1) and the interface formation model (curve 2) with experiments from Paulsen *et al.* (2011) (error bars) and Thoroddsen *et al.* (2005) (triangles), for (a) $Re = 1.4 \times 10^4$, (b) $Re = 68$ and (c) $Re = 2.9$. Curves marked with a prime are those computed for each model when the gas is considered passive.

scales recovered are much larger than the relaxation time of the interface, which would be an obvious initial estimate for these scales. The cause of this phenomenon has not been fully accounted for, but it appears to be related to the unsteady nature of the process, with rapid variations in the shape of the interfaces, combined with the initial far-from-equilibrium configuration of the system. When combined, these effects sustain the non-equilibrium interfacial dynamics. What would be of particular interest is the development of an asymptotic theory for the different stages of the

process, which may shed additional light on how the interface is maintained in its non-equilibrium state. Furthermore, such a theory, or scaling law, could make a comparison of the interface formation theory with experimental data a more routine task, rather than requiring full computation at every stage.

So far, we have focused on the dynamics of the bridge of a millimetre-sized drop, where we saw that the results obtained in the framework of different models for the bridge dynamics on the microscale differ significantly, but these differences do not affect the global dynamics of the drops, as the interface formation/disappearance processes are over long before the global dynamics comes into play. In contrast, in §5.4 we saw that for a micro-drop the global dynamics of the drop is heavily dependent on the model used. Consequently, theory-driven experiments in this range can target global features of the drop coalescence process such as, say, the aspect ratio of the drop, as often used to characterize oscillating drops (Sprittles & Shikhmurzaev 2012*b*). In this way, by studying smaller drops, optical measurement again becomes a viable method for probing the physics of the coalescence process.

Acknowledgements

The authors would like to thank Dr J. D. Paulsen, Dr J. C. Burton and Professor S. R. Nagel for providing us with the data from their experiments published in Paulsen *et al.* (2011) and Dr Y. Li for spotting the typographical error in Sprittles & Shikhmurzaev (2013).

Appendix A. Correction to Sprittles & Shikhmurzaev (2013)

Since publishing our user-friendly step-by-step guide to the finite element implementation of the interface formation model in the Appendix of Sprittles & Shikhmurzaev (2013), a typographical error has been brought to our attention, which is present in the text, but not in the code that has been developed. In particular, equation (53) there should read

$$\nabla^s \cdot \mathbf{a}^s = \frac{\partial a_t^s}{\partial s} + \frac{na_{t,r}^s}{r}, \quad a_{t,r}^s = (\mathbf{a}^s \cdot \mathbf{t})(\mathbf{t} \cdot \mathbf{e}_r) \quad (\text{A } 1)$$

and, consequently, the second term on the right-hand side of equation (63) there should be changed from

$$n\rho_{\gamma,j}^s \frac{dr_{\gamma,k}}{dt} \int_{s_{\gamma e}} \phi_{\gamma,i} \phi_{\gamma,j} \phi_{\gamma,k} ds_{\gamma,e} \quad \text{to} \quad n\rho_{\gamma,j}^s c_{t,k}^s \int_{s_{\gamma e}} \phi_{\gamma,i} \phi_{\gamma,j} \phi_{\gamma,k} t_r ds_{\gamma,e}, \quad (\text{A } 2a,b)$$

with resulting expressions altered accordingly. It is important to stress that the correct equations were always used in our code.

REFERENCES

- AARTS, D. G. A. L., LEKKERKERKER, H. N. W., GUO, H., WEGDAM, G. H. & BONN, D. 2005 Hydrodynamics of droplet coalescence. *Phys. Rev. Lett.* **95**, 164503.
- BELLEHUMEUR, C. T., BIARIA, M. K. & VLACHOPOULOS, J. 2004 An experimental study and model assessment of polymer sintering. *Polym. Engng Sci.* **36**, 2198–2207.
- BLAKE, T. D. & SHIKHMURZAEV, Y. D. 2002 Dynamic wetting by liquids of different viscosity. *J. Colloid Interface Sci.* **253**, 196–202.

- DERBY, B. 2010 Inkjet printing of functional and structural materials: fluid property requirements, feature stability and resolution. *Annu. Rev. Mater. Res.* **40**, 395–414.
- DREHER, T. M., GLASS, J., O'CONNOR, A. J. & STEVENS, G. W. 1999 Effect of rheology on coalescence rates and emulsion stability. *AIChE J.* **45**, 1182–1190.
- DUCHEMIN, L., EGGERS, J. & JOSSERAND, C. 2003 Inviscid coalescence of drops. *J. Fluid Mech.* **487**, 167–178.
- EGGERS, J., LISTER, J. R. & STONE, H. A. 1999 Coalescence of liquid drops. *J. Fluid Mech.* **401**, 293–310.
- GRISSOM, W. M. & WIERUM, F. A. 1981 Liquid spray cooling of a heated surface. *Intl J. Heat Mass Transfer* **24**, 261–271.
- HOPPER, R. W. 1984 Coalescence of two equal cylinders: exact results for creeping viscous plane flow driven by capillarity. *J. Am. Ceram. Soc.* **67**, 262–264.
- HOPPER, R. W. 1990 Plane Stokes flow driven by capillarity on a free surface. *J. Fluid Mech.* **213**, 349–375.
- HOPPER, R. W. 1993a Coalescence of two viscous cylinders by capillarity: part 1. Theory. *J. Am. Ceram. Soc.* **76**, 2947–2952.
- HOPPER, R. W. 1993b Coalescence of two viscous cylinders by capillarity: part 2. Shape evolution. *J. Am. Ceram. Soc.* **76**, 2953–2960.
- KOVETZ, A. & OLUND, B. 1969 The effect of coalescence and condensation on rain formation in a cloud of finite vertical extent. *J. Atmos. Sci.* **26**, 1060–1065.
- OGUZ, H. N. & PROSPERETTI, A. 1989 Surface-tension effects in the contact of liquid surfaces. *J. Fluid Mech.* **203**, 149–171.
- PAULSEN, J. D., BURTON, J. C. & NAGEL, S. R. 2011 Viscous to inertial crossover in liquid drop coalescence. *Phys. Rev. Lett.* **106**, 114501.
- RICHARDSON, S. 1992 Two-dimensional slow viscous flows with time-dependent free boundaries driven by surface tension. *Eur. J. Appl. Maths* **3**, 193–207.
- SEEMAN, R., BRINKMANN, M., PFOHL, T. & HERMINGHAUS, S. 2012 Droplet based microfluidics. *Rep. Prog. Phys.* **75**, 016601.
- SHIKHMURZAEV, Y. D. 1996 Spreading of drops on solid surfaces in a quasi-static regime. *Phys. Fluids* **9**, 266–275.
- SHIKHMURZAEV, Y. D. 2007 *Capillary Flows with Forming Interfaces*. Chapman & Hall/CRC.
- SINGH, M., HAVERINEN, H., DHAGAT, P. & JABBOUR, G. 2010 Inkjet printing process and its applications. *Adv. Mater.* **22**, 673–685.
- SPRITTLES, J. E. & SHIKHMURZAEV, Y. D. 2012a Coalescence of liquid drops: different models versus experiment. *Phys. Fluids* **24**, 122105.
- SPRITTLES, J. E. & SHIKHMURZAEV, Y. D. 2012b The dynamics of liquid drops and their interaction with solids of varying wettabilities. *Phys. Fluids* **24**, 082001.
- SPRITTLES, J. E. & SHIKHMURZAEV, Y. D. 2012c A finite element framework for describing dynamic wetting phenomena. *Intl J. Numer. Meth. Fluids* **68**, 1257–1298.
- SPRITTLES, J. E. & SHIKHMURZAEV, Y. D. 2013 Finite element simulation of dynamic wetting flows as an interface formation process. *J. Comput. Phys.* **233**, 34–65.
- SPRITTLES, J. E. & SHIKHMURZAEV, Y. D. 2014 A parametric study of the coalescence of liquid drops in a viscous gas. *J. Fluid Mech.* (submitted).
- SQUIRES, T. M. & QUAKE, S. R. 2005 Microfluidics: fluid physics at the nanoliter scale. *Rev. Mod. Phys.* **77**, 977–1026.
- THORODDSEN, S. T., TAKEHARA, K. & ETOH, T. G. 2005 The coalescence speed of a pendent and sessile drop. *J. Fluid Mech.* **527**, 85–114.
- WU, M., CUBAUD, T. & HO, C. 2004 Scaling law in liquid drop coalescence driven by surface tension. *Phys. Fluids* **16**, 51–54.
- YOUNG, T. 1805 An essay on the cohesion of fluids. *Phil. Trans. R. Soc. Lond.* **95**, 65–87.